

AD-A100 549 FOREIGN TECHNOLOGY DIV WRIGHT-PATTERSON AFB OH
LASER JOURNAL (SELECTED ARTICLES, (U)
MAY 81 Y WENYAN, W CHUANBAO, Y GONG
UNCLASSIFIED FTD-ID(RS)T-0121-81

F/G 20/5

NL

| or |
AD
A 00549

END
DATE
FILED
7-8-81
DTIC

ADA100549

2
~ FTD-ID(RS)T-0121-81

FOREIGN TECHNOLOGY DIVISION

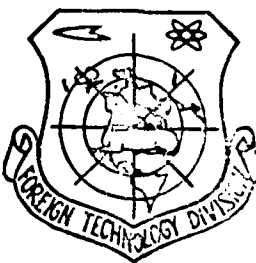


LASER JOURNAL
(Selected Articles)

DTIC

RECORDED

JUN 24 1981



Approved for public release;
distribution unlimited.

DTIC FILE COPY

4

81 6 23 042

FTD-ID(RS)T-0121-81

EDITED TRANSLATION

14 | FTD-ID(RS)T-0121-81

21 May 1981

MICROFICHE NR: FTD-81-C-000436

LASER JOURNAL (Selected Articles)

English pages: 33

Source: Laser Journal, Vol. 7, No. 9, 1980,
pp. 1-6, 21-26

Country of origin: China

Translated by: SCITRAN

F33657-78-D-0619

Requester: FTD/TQTD

Approved for public release; distribution
unlimited.

X

14/7/81

WU / 1-6, 21-26

Yu / 1-6, 21-26

Approved for public release	Approved for distribution
FTD	1981
A	

THIS TRANSLATION IS A RENDITION OF THE ORIGINAL FOREIGN TEXT WITHOUT ANY ANALYTICAL OR EDITORIAL COMMENT. STATEMENTS OR THEORIES ADVOCATED OR IMPLIED ARE THOSE OF THE SOURCE AND DO NOT NECESSARILY REFLECT THE POSITION OR OPINION OF THE FOREIGN TECHNOLOGY DIVISION.

PREPARED BY:

TRANSLATION DIVISION
FOREIGN TECHNOLOGY DIVISION
WPAFB, OHIO.

FTD-ID(RS)T-0121-81

Date 21 May 1981

TABLE OF CONTENTS

High Power Multi-Pass Amplifier, by Fan Dianyuan, Yu Wenyang.....	1
Study on the Arrayed Nozzles for Gas-Dynamic Lasers, by Wu Chuanbao, Yu Gong.....	18

HIGH POWER MULTI-PASS AMPLIFIER

Fan Dianyuan
Yu Wenyuan

(Shanghai Institute of Optics and Fine Mechanics, Academia Sinica)

Abstract

The gain of a high power multi-pass amplifier is studied. The conditions for raising the energy extracting efficiency are discussed. We obtain the general rule to select the optimum parameters. This result has been used to build a disk amplifier; there are three optical paths in the amplifier; and the laser beam of 100 mm aperture passes through it six times, back and forth. Theoretical calculations are in agreement with the experimental results.

I. THE ENERGY AND GAIN OF A HIGH POWER MULTI-PASS AMPLIFIER

The operation of a laser beam passing through an amplifier several times is called multi-pass amplification. The purpose of studying multi-pass amplification is threefold. Firstly, the operation can effectively upgrade the efficiency of the amplifier. Secondly, in a laser-induced nuclear fusion experiment, the target-reflected laser will return to the amplification system. Therefore, it is very important to evaluate the gain and energy of the reflected laser. This is a typical double-pass amplification

Received September 18, 1979

problem. Thirdly, the amplification of a pulse array can be treated essentially as a multiple-pass problem.

The laser pulse being studied operates in the nano-second and sub-nanosecond range. The classical theory and simplified three energy level model can be used to calculate the gain. Then, the variation of energy density of the laser beam in the amplifier is determined by the following equation:

$$\frac{dE}{dz} = E_s B_0 [1 - e^{-E/E_s}] - \alpha E, \quad (1)$$

where $E(z)$ is the energy density of the laser beam (joules/cm^2); $B_0(z) = \alpha N_0(z)$ is the initial gain coefficient (cm^{-1}); $E_s = h\nu/2\sigma$ is the saturated energy density (joules/cm^2); α is the absorption coefficient (cm^{-1}).

This is a non-linear equation which must in general be solved with the help of a computer. We have been observing the effects of light absorption, transverse isotropy and light beam divergence on the gain. Based on those effects, we determined the accuracy and application range for many approximate analytical formulas, such as "concentrated loss approximation", "uniform distribution approximation", "equi-efficiency absorption coefficient," etc. This article will concentrate on the discussion of the gain problem of multi-pass amplification.

In order to calculate the gain of a light beam passing the amplifier each time, the key problem will be to understand fully the variation rule for the density of reversed particles. This is different from the case of single-pass amplification. It is not only controlled by the excited transition, but it is also related to the relaxation effect between energy levels. The excited transitions dominate at the moment when light beams pass the amplifier, while during the time interval between the departure

of the prior laser and the arrival of the incoming laser, the relaxation effect is a decisive factor.

We first discuss the significance of the relaxation effect. In neodymium glass, there are two categories for the relaxation between energy levels: one is the "thermalization" of sublevels, metastable state ($^4F_{3/2}$) and final state ($^4I_{11/2}$), i.e. the particle spontaneously tends to reach the thermal equilibrium distribution; the other category is the vacant final state, i.e. the particle in the $^4I_{11/2}$ state spontaneously transfers to the ground state. The energy level structures of three types of neodymium glasses manufactured in China are shown in Figure 1. In thermal equilibrium, the number of particles at a sublevel follows the Boltzmann distribution. For a metastable state, the following relation is obtained:

$$\bar{n}_e = k_2 \bar{n}_b, \quad k_2 = 0.434. \quad (2)$$

For the energy level of a final state, the relation is:

$$\begin{aligned} \bar{m}_e &= k_1 \bar{m}_b, \\ k_1 &= 0.619 + 0.404 + 0.286 \\ &\quad + 0.202 + 0.140 = 1.651_c \end{aligned} \quad \left. \right\} \quad (3)$$

When the particle distribution deviates from the equilibrium state, under certain external influences, the relaxation will restore the equilibrium. The rate of the recovery can be described phenomenologically by a characteristic time, i.e. the thermalization time of the sublevel T . The value of T is roughly on the order of 10 ns [1]. On the other hand, the evacuation rate of the particle number at the final state level is described by the lifetime of the final state τ . Various measurements on τ have been reported, generally in the range of ten to one hundred nano-seconds [2].

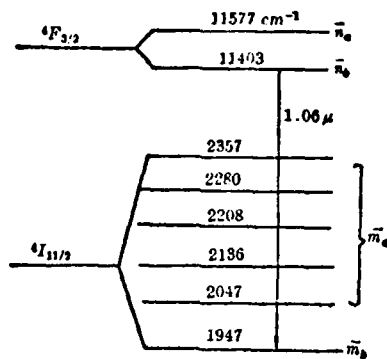


Figure 1. Energy level structure of the N_{0312} neodymium glass.

As a result, the particle density at any sublevel will vary with time in accordance with the following equations.

For metastable state:

$$n(t) = \bar{n} + [n(0) - \bar{n}] e^{-t/\tau}, \quad (4)$$

For final state:

$$m(t) = \{\bar{m} + [m(0) - \bar{m}] e^{-t/T}\} e^{-t/\tau} \quad (5)$$

where $n(0)$, $m(0)$ are particle densities at $t = 0$, \bar{n} , \bar{m} are the values at thermal equilibrium, which are determined by Equations (2) and (3). The lifetime of the metastable state is not taken into account in Equation (4), simply because it lasts for several hundreds of micro-seconds and does not affect the multi-pass amplification process significantly.

It is easy to calculate the variation of particle distribution induced by excited transitions. Assume the initial reversed particle density to be N_o , then the density of residual reversed

particles after amplification can easily be derived by the speed equation, leading to:

$$N(Z) = N_0(Z) e^{-\frac{E(Z)}{E_0}}. \quad (6)$$

Thus the particle density at upper energy level has been reduced by Δ :

$$\Delta = \frac{N_0 - N}{2} = \frac{N_0}{2} [1 - e^{-\frac{E}{E_0}}]. \quad (7)$$

Combining the results of excited transitions and relaxation effect, a general rule for variation of particle density during the entire process of multi-pass amplification can be set up. Suppose that the particle density distribution in material is described by the following four quantities prior to the k -th amplification:

N_0' -- the difference of particle densities at upper and lower working energy levels, $(n' - m')$;

S_0' -- the sum of particle densities at upper and lower working energy levels, $(n' + m')$;

S_2' -- the sum of particle density at each sub-level in the metastable state;

S_1' -- the sum of particle density at each sub-level in the final state.

The particle densities, after consecutive processes of amplification and relaxation and before the $(k+1)$ -th amplification, will be changed respectively to:

$$N''_0(\delta), S''_0(\delta), S''_2(\delta), S''_1(\delta).$$

where δ is the time interval between the two amplifications. According to the formula previously derived and referring to Figure 2, the following relations are obtained:

$$\left. \begin{aligned} N''(\delta) &= \left[\frac{N'_0}{2} (1 + e^{-\delta/T}) + \frac{s'_0}{2} (1 - e^{-\delta/T}) \right] e^{-\delta/T} + \left[\frac{s'_2}{1+k_2} - \frac{s'_1}{1+k_1} e^{-\delta/T} \right] (1 - e^{-\delta/T}) \\ &\quad - \Delta' (A_2 + A_1 e^{-\delta/T}), \\ s''_0(\delta) &= \left[\frac{N'_0}{2} (1 - e^{-\delta/T}) + \frac{s'_0}{2} (1 + e^{-\delta/T}) \right] e^{-\delta/T} + \left[\frac{s'_2}{1+k_2} + \frac{s'_1}{1+k_1} e^{-\delta/T} \right] (1 - e^{-\delta/T}) \\ &\quad - \Delta' (A_2 - A_1 e^{-\delta/T}), \\ s''_2(\delta) &= s'_2 - \Delta', \\ s''_1(\delta) &= (s'_1 + \Delta') e^{-\delta/T} \end{aligned} \right\} \quad (8)$$

where

$$A_1 = \frac{1+k_1 e^{-\delta/T}}{1+k_1},$$

$$A_2 = \frac{1+k_2 e^{-\delta/T}}{1+k_2},$$

and Δ' is given in Equation (6).

$$\begin{array}{ccc} \text{A) } \frac{s' - n'}{n'} & \text{B) } \frac{s'_1 - n'}{n' - \Delta'} & \text{C) } \frac{s''_1 - n''(\delta)}{n''(\delta) = n'' + (n' - A - \bar{n}'') e^{-\delta T}} \\ \frac{s'_1 - m'}{m'} & \frac{s'_1 - m''(\delta)}{m''(\delta) = [\bar{m}'' + (m' + \Delta - \bar{m}'') e^{-\delta T}] e^{-\delta T}} & \end{array}$$

Figure 2. Variation of particle distributions: A) initial distribution; B) variation induced by excited transitions; C) variation induced by relaxation after a time interval,

This is a set of recurrence relations. Once the initial particle density and input laser energy density at each pass are given, the reversed particle density and energy gain after any amplification can be calculated. Equation (8) is a general formula which can be applied to any situation in practical operations. The formula also covers many special results derived in

previous articles.

Since the practical implication of the double-pass amplification is more extensive than others, and the approximate solution can be obtained, we will discuss double-pass amplification in more detail.

It can reasonably be assumed that the initial reversed particle density in the operating material is uniformly distributed before the first laser train enters the amplifier. In addition, the final state is nearly evacuated, and the energy levels in the metastable state are thermalized. Then, the initial conditions will be:

$$s'_0 = N'_0, \quad s'_1 = 0, \quad s'_2 = (1+k_2)N'_0 \quad (9)$$

The recurrence relation, Equation (8), can be amplified to:

$$\left. \begin{array}{l} N''_0(\delta) = N'_0 - (A_2 + A_1 e^{-\delta/\tau}) \Delta', \\ s''_0(\delta) = N'_0 - (A_2 - A_1 e^{-\delta/\tau}) \Delta', \\ s''_2(\delta) = (1+k_2)N'_0 - \Delta', \\ s''_1(\delta) = \Delta' e^{-\delta/\tau}. \end{array} \right\} \quad (10)$$

Thus, the gains in the first round and the second round can be represented by the following expressions:

$$\begin{aligned} G'(L) &= \frac{E'(L)}{E'_0} \\ &= \frac{E_s}{E'_0} \ln [1 + (e^{E_s - E_0} - 1) g'_0] e^{-\alpha L}, \end{aligned} \quad (11a)$$

$$\begin{aligned} G''(L) &= \frac{E''(L)}{E''_0} \\ &= \frac{E_s}{E''_0} \ln [1 + (e^{E_s - E_0} - 1) g''_0] e^{-\alpha L}. \end{aligned} \quad (11b)$$

where E'_0 , E''_0 are energy densities of input light at first and second passes, respectively; $E'(L)$, $E''(L)$ are energy densities of light at the output terminal of the amplifier; ξ'_0 , ξ''_0 are small signal gains in the first and second amplifications, which are defined as:

$$g'_0 = e^{\alpha N_0 L}, \quad (12a)$$

$$\begin{aligned} g''_0 &= e^{\alpha \int_0^L N_0 dZ} \\ &= g'_0 \exp \left\{ \frac{-A}{2E'_0} [E'(L) - E'_0 \right. \\ &\quad \left. + \alpha \int_0^L E'(Z) dZ] \right\}. \end{aligned} \quad (12b)$$

Equations (10), (11), (12) are complete solutions for the double-pass amplification problem. The parameter $A = A_2 + A_1 e^{-\delta/\tau}$ represents the influence of the relaxation effect, which varies with the time interval δ . The following table lists several typical cases.

δ	$\delta \ll T$	$\delta \approx T$	$T < \delta \ll \tau$	$\delta \approx \tau$	$\delta \gg \tau$
Relaxation degree	Thermalization and evacuation are neglected	Basic thermalization; evacuation is neglected	Full thermalization; basic evacuation	Full thermalization; full evacuation	
A	2	1.412	1.047	0.835	0.696

A practical example for the double-pass amplification is given in the third section of this article.

We will study the amplification problem for pulse series in the following. The physical process and calculation method are basically no different from the double-pass amplification.

However, the number of pulses is much greater; hence, the expression is more tedious for calculating the gain of every pulse. Accordingly, the optimum expression will be the recurrence relation. Besides, the interval between pulses is usually shorter ($\delta/\tau \ll 1$) ; hence, the evacuation effect of the final state may not be considered. Consequently, the variation of particle numbers must be described by three quantities. The recurrence relation Equation (8) is reduced to:

$$N_0^{(k)} = N_0^{(k-1)} e^{-\delta T} + \left[\frac{s_2^{(k-1)}}{1+k_2} - \frac{s_1^{(k-1)}}{1+k_1} \right] \times (1 - e^{-\delta T}) - \Delta^{(k-1)}(A_2 + A_1),$$

$$s_2^{(k)} = s_2^{(k-1)} - \Delta^{(k-1)},$$

$$s_1^{(k)} = s_1^{(k-1)} + \Delta^{(k-1)}.$$

The following initial conditions are given:

$$g_0^{(1)} = e^{\sigma \int_0^T N_0^{(1)} dz}, \quad s_1^{(1)} = 0, \quad s_2^{(1)} = (1+k_2) N_0^{(1)},$$

The small signal gain, $g_0^{(k)}$, and energy density of output light, $E^{(k)}(L)$, of any pulse can be derived, leading to:

$$g_0^{(k)} = e^{\sigma \int_0^T N_0^{(k)} dz},$$

$$E^{(k)}(L) = E_0 \ln [1 + (e^{F^{(k)} / E_0} - 1) g_0^{(k)}] e^{-\alpha L}.$$

The above formulas apply to any case which satisfies $\delta/\tau \ll 1$. It is not difficult to prove that the above formulas are reduced to the results derived in Ref. 2 for the special case of $\delta/T \gg 1$ and $\alpha = 0$.

II. THE ENERGY EXTRACTION EFFICIENCY OF A HIGH POWER AMPLIFIER

Energy conversion efficiency is an important characteristic

indicator of an amplifier. We will not discuss here the problem related to light pumping efficiency, but we will study the efficiency of storage energy of initial reversed particles converted to laser energy -- extracting energy. The so-called "extraction laser energy" means the difference between the output and input light energies of an amplifier. It equals the light energy released through excited transitions after subtracting the energy loss of operating materials. For convenience, we define a local extraction efficiency $\eta(z)$ and a total extraction efficiency $\bar{\eta}$:

$$\eta(z) = \frac{\text{extraction energy density at point } Z \text{ in the amplifier}}{\text{storage energy density at point } Z}$$

$$= \frac{h\nu(n_{30} - n_3) - \alpha E}{h\nu N_0} \quad (13)$$

$$\bar{\eta} = \frac{\text{total extraction energy in an amplifier}}{\text{total storage energy}}$$

$$= \iint (E_L - E_0) dS / \iint \left(\int_0^L h\nu N_0 dZ \right) dS \quad (14)$$

where n_{30} is the density of the initial particles in the metastable state; n_3 is the density of remaining particles in the metastable state after the laser beam passes; N_0 is the density of initial reversed particles; E_L , E_0 are densities of output and input light energies, respectively.

The total extracting efficiency can also be rewritten in the form:

$$\bar{\eta} = \frac{\iint \left(\int_0^L \eta(Z) N_0(Z) dZ \right) dS}{\iint \left(\int_0^L N_0(Z) dZ \right) dS}$$

It can be seen that $\bar{\eta}$ is the mean value of $\eta(Z)$.

We first discuss the local extraction efficiency problem. $\eta(Z)$ can be expressed, using Equation (1), as the following:

$$\eta(Z) = \frac{1 - e^{-E(Z)/E_0}}{2} - \frac{1}{2} \frac{\alpha}{\beta_0} \frac{E(Z)}{E_0} \quad (15)$$

where $E(Z)$ is a variable, β_0/α is a parameter, and the variation rule of $\eta(Z)$ is shown in Figure 3. The curves in the figure reflect the fundamental characteristics of extraction efficiency. As can be seen, for any given energy density, extraction efficiency increases with increasing β_0/α . As a result, the intense light pumping is in general advantageous for upgrading efficiency. Secondly, for a given β_0/α , there exists a maximum on each curve. Thus, in order to achieve a high efficiency, the operating region in an amplifier (i. e. the variation range from input energy density, E_0 , to output energy density, E_L) must be located near the maximum. The efficiency can be reduced when light energy density is too large or too small. The light energy density corresponding to the maximum, E_m , can easily be derived:

$$E_m = E_0 \ln(\beta_0/\alpha).$$

The value of β_0/α mostly observed in experiments is around 10. The corresponding E_m is over double the saturated energy density E_s , which far exceeds the loading capability of neodymium glass. Thus, the condition for optimum operating region is hardly realized. In the following, we will study a problem which has a practical significance: how to increase extraction efficiency without increasing light energy density. Assuming that the transverse distribution is uniform, the total extraction efficiency can be reduced to:

$$\bar{\eta} = (E_L - E_0) / 2E_0\beta_0 L \quad (16)$$

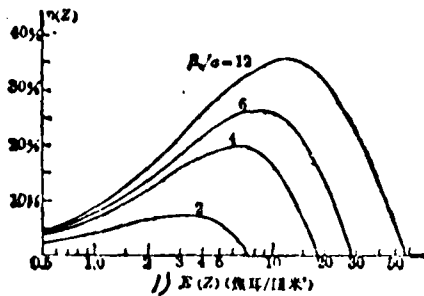


Figure 3. Local extraction efficiency.

1) $E(Z)$ (joules/cm³)

There are four variables affecting $\bar{\eta}$: E_1 , E_0 , β_0 , L , but only three of them are independent through Equation (1). To be explicit, Equation (1) can be transformed into the following expression:

$$L = \int_{E_0}^{E_1} dE / [E_s \beta_0 (1 - e^{-E/E_s}) - \alpha E], \quad (17)$$

which is substituted into Equation (16) to result in:

$$\bar{\eta} = (E_1 - E_0) / 2E_s (\beta_0/\alpha) \int_{E_0}^{E_1} dE / [E_s (\beta_0/\alpha) (1 - e^{-E/E_s}) - E]. \quad (18)$$

When the operating region is determined, $\bar{\eta}$ varies with β_0/α . It can be proved that only if $E_1 > E_0$, $\frac{d\bar{\eta}}{d(\beta_0/\alpha)} > 0$. Is it always effective. That is, $\bar{\eta}$ increases with increasing β_0/α . When $\beta_0/\alpha \rightarrow \infty$, $\bar{\eta}$ approaches a maximum $\bar{\eta}_m$:

$$\bar{\eta}_m = (E_1 - E_0) / 2E_s \ln [(e^{E_1/E_s} - 1) / (e^{E_0/E_s} - 1)]. \quad (19)$$

Several sets of $\bar{\eta} - \beta_0/\alpha$ relation curves are shown in Figure 4, calculated for several popular experimental environments. Those curves indicate that an upgrading of β_0/α will enhance the efficiency. It is particularly prominent when β_0/α is small. But when β_0/α approaches 10, it will be close to the maximum extraction efficiency, and any further increase in β_0/α cannot help the efficiency significantly. Consequently, how to choose β_0/α

value properly is a critical problem needed to be taken into account in amplifier design.

When the β_0/a is given, the length of the amplifier cannot be random in order to satisfy the input and output requirements. The length is determined by Equation (17). It can easily be seen that L decreases with increasing β_0 . Subject to the limitation of amplifier loading, we should adopt intense light pumping (large β_0 and short bar (small L)) along with a value of β_0/a no greater than 10, in order to achieve a high efficiency.

III. TWO ROUND, THREE PASS DISK AMPLIFIER

We designed and developed a large-scale disk amplifier as an application of the foregoing theory. The amplifier is composed of six slices of neodymium glass; each slice has a thickness of 35 mm, width of 180 mm, height of 300 mm. The slice is inclined at a Bragg's angle ($56^{\circ}24'$). The dimensions of the light pass aperture are 100 mm x 300 mm. The amplifier also includes 12 upright xenon lamp light pumps as shown in Figure 5. The light beam passes the lower, middle and upper parts consecutively, thus

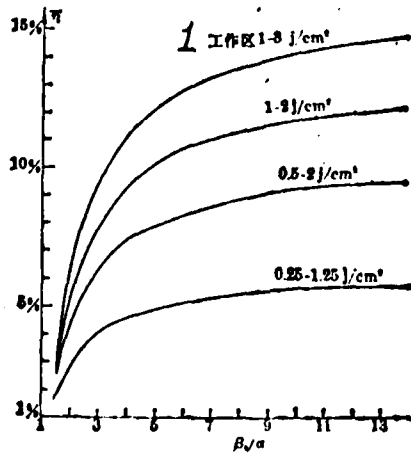


Figure 4. The relation between total extraction efficiency and β_0/a . Key: 1) operating region.

forming three passes. In order to raise the gain and efficiency, another passage is repeated. Figure 5(B) shows the light paths following the principle of two round, three pass operation. In order to fully utilize the advantages of double-pass amplification and final state evacuation effect, the time interval between the two consecutive rounds of amplification must be as large as possible. Consequently, the distance between reflection mirrors is about 15 m, and $\delta \approx \pi$ is taken for calculation of the gain in the second round of amplification.

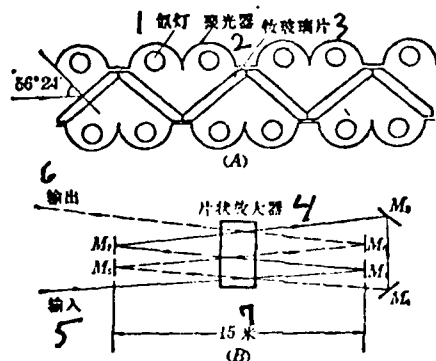


Figure 5. Disk amplifier: A) structure; B) conceptual light paths; 1) xenon lamp; 2) light concentrator; 3) neodymium glass slice; 4) disk amplifier; 5) input; 6) output; 7) 15 m.

The static absorption coefficient of the neodymium glass is $\alpha_0 = 0.16\%$. However, for light pumping operation, the dynamic absorption for the $1.06 \mu\text{m}$ laser is larger than α_0 (about two to three times α_0) because of the upward excited transitions of instantaneous color centers and metastable states, as well as the nonlinear absorption during intense laser interaction. We take the absorption coefficient to be $\alpha = 2.5\alpha_0 = 0.4\%$.

Surface loss is determined by experiments. The total loss of each neodymium glass slice thus obtained is 2%.

The initial gain coefficient is derived from small-scale simulated experimental data. When the density of light pumping (electric energy/neodymium glass volume) is 29 joules/cm^3 , $\beta_0 = 2.86\% \text{ cm}^{-1}$.

In accordance with formulas previously derived, we calculate, for a typical case with input laser energy of 40 joules, the gain and output energy of each round of amplification which is listed in the following table:

	Energy Gain	Output Energy	Average Residual at Reversed Number	Footnotes
First round	4.24 times	172 joules	85%	Diameters of light beam are $\frac{1}{2}70$, 80, and 90, respectively
Second round	2.50	430	64%	Diameter of light beam is $\frac{1}{2}100$
Total of two rounds	10.6	430	64%	
Reversed later	3.01	127		Reflectivity of target surface is 10%

The experimental results are: input energy 40 joules, output energy 399 joules, gain 10. Experimental values and values obtained by theoretical calculations are basically in agreement.

The disk amplifier is intended for use in a nuclear fusion experiment, hence the table also lists some calculated results for the gain of the reversed laser. In the calculation, we assume the retardation rate of each pass as 8%. Experimental values are in agreement with calculated values.

In order to further examine the theory, we have conducted measurements and theoretical calculations of gains for various energies of light pumping and various laser intensities. The results are listed in the following table.*

Series #	Density of Light Pumping	Input Laser Energy	Gain Coefficient	Calculated Values for Gain	Experimental Values
1	11.4 joules/cm ³	44.5 joules	1.37% cm ⁻¹	2.30 times	2.80 times
2	11.4	50.5	1.37%	2.23	2.76
3	16.4	62.0	1.88%	3.64	3.98
4	23.6	53.5	2.54%	7.05	7.00
5	26.2	44.0	2.71%	9.06	8.40
6	29.0	40.0	2.86%	10.6	9.97

The results indicate that under various operating conditions the calculated values are basically in agreement with experiments.

Finally, we want to examine the problem with respect to the efficiency of energy conversion. When the density of light pumping is 29 joules/cm³, the total input electric energy is 3.6×10^5 joules, and the total extraction laser energy in two rounds of amplifications is 360 joules, thus leading to a total efficiency of 0.1%. The efficiency of electric energy converted to the storage energy of

NOTE: The gain coefficient is not simply proportional to the light pumping energy. The effect due to the variation of light emission of a xenon lamp must be taken into account.

reversed particles (i.e. the efficiency of light pumping) is 0.89%, and the extraction efficiency is 11.2%. Compared to other similar types of amplifiers, the extraction efficiency is higher for this case due to the use of the double-pass amplification along with a higher energy density of the light beam. The C series disk installed in the Cyclops at Livermore Laboratory in the United States has a light pumping efficiency of close to 1%. However, the energy density of the light beam can be controlled only in the range of a small signal, due to the restriction of the nonlinear effect. Thus, the extracting efficiency is very low, only about 1%. It is expected that, if our device is applied to the amplification of picosecond pulses, the efficiency will decline.

The foregoing discussions imply that, in order to achieve higher efficiency, research on high-power amplifiers must result in the improvement of light beam transmission conditions and overcoming the nonlinear restriction so as to raise the loading capability of operating materials as much as possible. It is wise to emphasize light pumping.

REFERENCES

- [1] P. G. Magnante; *IEEE J. Quant. Electr.*, 1972, **QE-6**, 440.
- [2] R. Dumanchin *et al.*; *IEEE J. Quant. Electr.*, 1971, **QE-7**, 53.
- [3] J. A. Glaze; *SPIE*, 1975, **69**, 45.

STUDY ON THE ARRAYER NOZZLES
FOR GAS-DYNAMIC LASERS

Wu Chuanbao
Yu Gong

(Institute of Mechanics, Academia Sinica)

Abstract

Based on practical work in 1971-1976, some problems to be considered in designing of rapid expansion nozzles for gas-dynamic lasers were summarized, including the selection of important parameters, the discussion on methods for contoured nozzles design and the correction for boundary layer growth, etc. Through a large amount of numerical analysis, a simple convenient method for correcting boundary layer growth under various conditions was also presented.

I. INTRODUCTION

The rapid expansion nozzle is a key component for the gas-dynamic laser. Its major function is to rapidly and effectively freeze the vibration energy in gas-dynamic operation. It is different from the conventional nozzle installed in a supersonic wind tunnel. The basic principle in designing a gas-dynamic nozzle in a laser device should be: only the premise guaranteeing an air current with minimum perturbation. Maximum freezing should

Received October 6, 1979

be achieved. The perturbation of an air current, i.e. the non-uniformity of an air current, will directly affect the quality of the output light beam, while the freezing effect is related to the efficiency of the device. There is some contradiction between guaranteeing a uniform air current and effective freezing. It requires overall balance and reasonable adjustment.

II. FACTORS WHICH AFFECT THE FREEZING EFFECTS OF A NOZZLE

A large amount of theoretical analysis and experimental studies have indicated [1-8] that, for a certain air current retardation condition, the major factor which affects the freezing is the geometry of the nozzle. Its primary geometrical parameters include curvature radii of the throat, R_1 and R_2 , the maximum expansion angle of the air current, θ_2 , the height of the throat pipe, R^* , and the area ratio, A_0/A^* (see Figure 1).

How the shape of a subsonic nozzle affects the freezing effect cannot be overlooked. A small curvature radius, R_1 , of the throat and a large entrance angle, θ_1 , for an air current enable the air current to become unbalanced in the subsonic range and this expedites the freezing of vibration energy. $R_1=0$ and $\theta_1=90^\circ$ represent the fastest subsonic expansion and the best freezing effect. But at $R_1=h^*$ and $\theta_1=45^\circ$, the degradation of quality is not very significant [6]. The curvature radius, R_2 , of the throat in the supersonic portion of a nozzle has the same influence on the freezing effect as R_1 . In principle, the smaller the better. Its value is determined by the calculation method for the contoured nozzle. In general, the minimum length of a nozzle is calculated by the method of characteristic lines with which the throat portion appears at an acute angle and $R_2=0$. If the Foelsch method is applied to calculating the nozzle [9,10], the curvature radius of the throat will be related to h^* and θ_2 . In general, $R_2 < h^*$. As for θ_2 , the maximum value of θ_2 allowed in the theory is generally taken, i.e. half of Prandtl-Meyer expansion angle ω_E ($\theta_2 = \frac{1}{2}\omega_E$) in designing Mach correspondence.

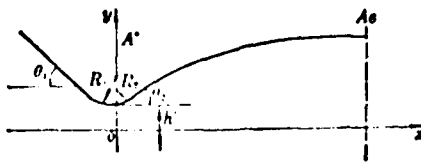


Figure 1. Geometrical parameters of a nozzle.

The height h^* of the nozzle throat is an important parameter which characterizes the freezing efficiency of the nozzle. For nozzles with the same area ratio (viscosity is not taken into account), the geometries are similar. The smaller the dimensions of the throat pipe, the shorter the length of the nozzle, and the variations of air current parameters along the axial direction are larger. Consequently, the freezing effect is more prominent. Small throat height is a characteristic of a nozzle of a gas-dynamic laser device, usually on the order of 0.5 mm. If manufacture and assembly can be warranted, and if the contour surface of the nozzle can be sufficiently cooled (especially in the throat region), the height of the throat can be further reduced, e. g. reduced to as small as 0.1 mm [11].

The ratio of the nozzle outlet area to the throat area A_0/A^* is another important parameter for determining the freezing efficiency of a nozzle. The larger the area ratio, the larger the degree of air current expansion, and the lower the temperature and pressure of the air current in the nozzle. In general, the area ratio is determined by the relation of equal entropy in accordance with the ratio of retarding temperature, T_o , accessible in the burning chamber to regulated temperature of the air current in a light cavity, T . The air current temperature in a light cavity is regulated to guarantee the vapor will not be condensed. In the past, $T \approx 300^{\circ}\text{K}$ was usually taken. But the vapor in a nozzle is not condensed immediately after saturation during the process of rapid expansion. It generally requires $40\text{--}80^{\circ}\text{C}$ excessive cooling temperature. In addition, part of vibration energy in $\text{CO}_2\text{-H}_2$ is

finally converted to kinetic energy through a relaxation process, leading to a higher air current temperature compared to the calculated temperature with the equal-entropy relation. Accordingly, by considering these two factors, the area ratio can be chosen larger.

In the discussion of factors which affect the freezing effect, the problem regarding the recombination parameter $p_0 h^*$ must be taken into account. Stollery and Smith [12] proposed a similar parameter $p_0 h^*$ to describe the freezing effect before, when they studied the non-equilibrium effect of a nozzle. Gerry[1] derived the fact that freezing usually occurs near the throat region. He derived a principle which describes the freezing effect of a gas-dynamic laser device, represented by $p_0 h^*$:

$$p_0 h^* < 2(p_{r_{th}}) T_{\infty} u^*$$

This principle was supported by Anderson [5]. He deliberated the implication of this recombination parameter and pointed out that if other parameters of the nozzle (such as gas components, temperature, area ratio, etc.) are invariant, the maximum gain and the maximum usable energy are all single-valued functions of $p_0 h^*$. He also suggested that it is more appropriate to take $p_0 h^* \approx 1$ atm. cm. We believe that this recombination parameter can be used as a reference in designing.

III. FACTORS WHICH AFFECT THE UNIFORMITY OF THE AIR CURRENT

There are many factors which affect the uniformity of the air current. For arrayed nozzles of a gas-dynamic laser device, major factors are wave series and tail trace. The tail of thin disks in the arrayed nozzles must be cut due to consideration of structure strength, thus inevitably generating excited waves of certain intensity. The air current through the tail will

generate fluctuating tail traces due to viscosity. Secondly, improper design of a nozzle (including correction of the viscosity effect) and improper assembly may induce air currents to generate various perturbations (air current separation, various degrees of expansion and compressed wave series, as well as the interaction between the wave series and boundary layer). In addition, the non-uniformity and instability of the initial current from the burning chamber, due to burning and mixing, must be taken into account.

Quantitative evaluation of the effect of these factors on the uniformity of air current is a difficult and complicated problem. To evaluate the effect of a non-uniformity of the air current incurred by these factors is even more difficult. We can only offer a crude qualitative introduction.

Simons[18] pointed out that, if the boundary layer on the side wall of the nozzle is not corrected, the excited waves induced by this type of boundary layer may make the air current generate a 10% density non-uniformity. A simple approach which enables side walls to expand outward linearly (precise quantity is determined by calculation, about on the order of $0.5 \sim 1^\circ$), can reduce such perturbations by more than half. Clark[14] estimated, with the method of geometrical optics, the effect of such perturbation on the quality of a light beam for a co-focus unstable cavity. When $\Delta\rho/\rho = 7\%$, remote fields parallel to and perpendicular to the air current are greatly deformed. In an analysis of this problem, Russell[15] pointed out that the density perturbation induced by excited waves near side walls must be limited to less than 1%.

For an excited wave intersecting the optical axis, it can only deflect light beams in general, i.e. the phase deviation is linear. The intensity of its remote field is unchanged relative to the deflected optical axis. Accordingly, such a deviation can be corrected through an external light path system. However, these

excited waves interact with tail trace or boundary layer, possibly leading to a high-order phase deviation. Therefore, the intensity of this type of excited waves must be reduced as much as possible.

Since the optical axis of gas-dynamic laser devices is arranged perpendicular to the rear part of the nozzle disk, the tail trace and fluctuating current do not affect the quality of the light beam very significantly[14]. They affect the quality of the light beam primarily through the divergency of the light beam. To properly evaluate these effects is very complicated.

The manufacture of nozzles, particularly those of the throat portion, must be accurate and provide excellent surface smoothness. Wagner[16] suggested that the accuracy in manufacturing must be guaranteed to ± 0.025 mm, and the surface smoothness must be 0.3×10^{-8} m (corresponding to $\nabla 11$). It can only be achieved through delicate grinding and projection. Currently we do not have technology to achieve that goal.

The assembly of nozzles, especially accurate dimensions of the throat portion, is very important. Since the dimensions of the throat portion are very small, a small assembly error (± 0.02) may lead to large relative error ($\pm 10\%$), hence seriously affecting the uniformity of the air current.

In order to have a uniform current, we must also assure the stability of nozzle dimensions during operation. As a result, nozzle cooling is a necessary step. In addition, because of the viscosity effect, the air current near the surface of the nozzle wall will be decelerated, converting the kinetic energy into thermal energy. The air current will be thereby heated and there may be an unfavorable impact on the reversal of particles. For a nozzle with $T_o = 1400$ K, $P_o = 25$ atm, $M = 4$, $h^* = 0.2$ mm, the loss of gain may reach 21%[11] when the temperature at the wall surface is $T_w = 700$ K.

Thus, from the viewpoint of freezing, the nozzle must be sufficiently cooled.

IV. DISCUSSIONS ON THE DESIGN OF NOZZLES

In order to reduce perturbations, a detailed gas-dynamical calculation of the nozzle wall is necessary. The guidelines in treatment of this problem may follow that of a nozzle installed in a conventional supersonic wind tunnel. Since the vibration energy is only a few percents of the total enthalpy, when the ratio of gas specific heats, γ , is given, the non-equilibrium effect can be neglected. The gas-dynamic parameters are not affected significantly if nozzle calculations are performed based on ideal air currents of equal entropy[11].

The design for the subsonic part is much easier. Only a linear contraction of nozzle areas and no counter-pressure in the axial direction need be assured. It is not necessary to calculate the wall shape in detail[15]. For example, even for the extreme case with entrance angle of $\theta_1 = 90^\circ$ and a curvature radius of the throat, $R_1 = 0$, air streams separation is not observed, and the requirement for the uniformity of the air stream is satisfied[6]. In addition, the air current subsonic part is very close to a one-dimensional current, only if $R_1 \neq 0$. Therefore, the linear contraction or wedge contraction, i.e. $\theta_1 = 45^\circ$, $R_1 \approx h^*$, are normally applied to the design of the subsonic unit.

For nozzles in the supersonic portion, reportedly the nozzle with minimum length calculated by the characteristic line method has been adopted in all cases [5, 6, 15, 16]. In the design, the throat portion is assumed to be a straight sonic line, and the initial expansion angle is taken as the maximum value, $\theta_2 = \frac{1}{2}\omega_E$. The throat pipe of this type of nozzle appears at an acute angle, along with maximum expansion speed and minimum length. In terms of freezing vibration energy, it is certainly a better design.

But there are problems in practice. Firstly, the requirements in manufacture and assembly are very strict. For an acute angle throat pipe, if the dislocation of the axial direction is 1% of throat height, a corresponding rotation angle perturbation of 1° in the air current is generated[15]. Secondly, the acute angle may easily cause separation of the air current, leading to rapid growth of the boundary layer on the side wall in the throat portion and generation of excited waves in the throat. The assumption of a straight sonic line also leads to over-expansion in the lower portion of the throat pipe, which may cause separation and generate excited waves. Accordingly, Anderson suggested using the arc shape to replace the acute angle. This approach may reduce theoretical gain and maximum usable energy by approximately 15%, but the real benefit may surpass it.

Consequently, the nozzle of minimum length designed by the characteristic line method is not a best one. We suggest that a method (Foelsch method) be employed which has been most popular in the design of conventional nozzles installed in a supersonic wind tunnel in China. The method assumes that the air current before the nozzle turning point has a spring current-like distribution. It is a very convenient analytical method which applies the principle of characteristic lines to calculate the nozzle well [10] as shown in Figure 2. Major formulas for calculation are listed below.

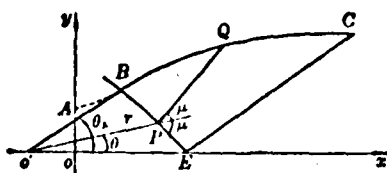


Figure 2. Design diagram of nozzle.

$$\begin{aligned} y_{B*} &= y_* + x_B \operatorname{tg} \theta_B \left(1 - \frac{1}{3} \frac{x}{x_B}\right) \left(\frac{x}{x_B}\right)^2 \\ x_{B*} &= r \cos \theta + Mr(\theta_B - \theta) \cos(\theta + \mu) - \overline{O'U} \end{aligned} \quad (1)$$

$$y_B = r \sin \theta + Mr(\theta_B - \theta) \sin(\theta + \mu) \quad (2)$$

$$\text{where } \theta_B = \frac{1}{2} \omega_{E_A} \quad \theta = \omega_B - \omega$$

$$\left. \begin{aligned} \omega &= \sqrt{\frac{\gamma+1}{\gamma-1}} \operatorname{tg}^{-1} \sqrt{\frac{\gamma-1}{\gamma+1} (M^2-1)} \\ &\quad - \operatorname{tg}^{-1} \sqrt{M^2-1} \\ r &= \frac{r_0}{M} \left[\frac{2}{\gamma+1} \left(1 + \frac{\gamma-1}{2} M^2 \right) \right]^{\frac{\gamma+1}{2(\gamma-1)}}, \\ r_0 &= y_* / \theta_B \\ \overline{O'U} &= r_B \cos \theta_B - x_B, \\ x_B &= \frac{3}{2} (r_B \cos \theta_B - y_* \operatorname{ctg} \theta_B) \\ \mu &= \sin^{-1} \frac{1}{M} \end{aligned} \right\} \quad (3)$$

The nozzle designed by the Foelsch method has a curvature radius in the throat portion of less than the throat height. The method takes care of requirements for freezing and uniformity of the air current. Besides, its wall coordinates are represented by simple analytical expressions which are convenient for various computations and analyses. This method provides adaptability of gas-dynamic laser nozzles, including higher Mach number and a larger expansion angle. Comparisons have been made with the characteristic line method by using electronic computers. Results indicate that, even though the spring current assumption has some discrepancies under this condition, the method is still usable. Results for practical operation of several types of gas-dynamic laser devices have indicated the following: the small signal gain measured has reached or even surpassed the best values of similar devices in other countries.

For gas-dynamic laser devices operated at low pressure, the density perturbation is not relatively serious because of the low cavity pressure. Thus the nozzle wall need not be carefully considered. Nozzles in simple wedge shape or cone shape can be used [15].

V. CALCULATIONS FOR FREEZING

For a gas-dynamic calculation, γ is a basic parameter. There are two viewpoints on γ . One regards that γ does not affect the theoretical wall significantly and $\gamma = 1.4$ can be assumed in designs. Its basic rationale is: once area ratios are identical, walls calculated by the same method but with different γ will not be much different. Another viewpoint is completely different. It considers γ value critical in wall calculations [15].

We believe that taking γ as a constant is an approximation, but we realize that γ affects the Mach number of the nozzle and the displacement thickness of boundary layer in some degree. On the other hand, it is inappropriate to choose a γ value randomly. Besides, the fact that nozzle wall coordinates are not significantly affected by the variation of γ may provide a basis for experiments to search for optimum parameters when gas components are changed in a fixed nozzle. However, such cases with optimum parameters usually do not apply to the case of nozzle design. In practical calculations, conceptual "freezing γ " may apply, i.e. assume that mixed air current is an equilibrium current before it flows through the throat pipe, while gas vibration energy is suddenly frozen in the throat pipe.

In consideration of the high characteristic temperature of two vibration energy levels ν_1, ν_2 for H_2O , the vibration energy for these two energy levels is negligible for a given retardation condition.

Thus, starting from the throat portion, only vibration energies of ν_1, ν_2 energy levels in CO_2 and ν_2 level in H_2O vary with the temperature of the air current in a mixed gas,

$$E_v(T) = E_{\text{vCO}_2}(\nu_1) + E_{\text{vCO}_2}(\nu_2) + E_{\text{vH}_2\text{O}}(\nu_2) \quad (4)$$

Since $E_v(T)$ is a function of temperature, the specific heat at constant volume C_v of the mixed gas (and thus γ) becomes a function of temperature. Accordingly, if γ is taken constant, we must find the average value of C_v in some sense.

Calculation steps are as follows:

- 1) Following the approach of equi-entropy variable specific heat, calculate the temperature of the air current, T_* , in the nozzle throat, which is used as the freezing temperature of upper energy levels of mixed gas, and is the initial temperature used to calculate the freezing γ .
- 2) Calculate the average value of C_v by applying the mean value theorem,

$$\begin{aligned} \bar{C}_v &= \frac{1}{T_e - T_*} \int_{T_*}^{T_e} (C_v)_{\nu} dT \\ &= \frac{1}{T_e - T_*} \int_{T_*}^{T_e} dE_v(T) \\ &= \frac{E_v(T_e) - E_v(T_*)}{T_e - T_*} \end{aligned} \quad (5)$$

where T_e is the air current temperature at the outlet of the nozzle.

- 3) Freezing γ can be calculated by the relation,

$$C_v = (C_v)_{Tr} + (\bar{C}_v)_v, \quad (6)$$

$$\gamma = 1 + \frac{R}{C_v}$$

where $(C_e)_r = \frac{5}{2} R(\psi_m + \psi_n) + 3R\psi_{n,0}$, R is the universal gas constant, ψ_i is the component.

VI. CALCULATIONS OF NOZZLE BOUNDARY LAYER

For rapid expansion nozzles in gas-dynamic laser devices, the development of the boundary layer in the axial direction of the nozzle is very fast because of the very small dimensions. As a result, the air current uniformity is substantially affected by viscosity.

Whether the boundary layer in the nozzle of a gas-dynamic laser device is laminar or turbulent is a problem bearing further discussion. In terms of the Reynolds number of a typical gas-dynamic laser nozzle (nozzle length is the characteristic length in this case), which is generally smaller than 10^6 , it should be laminar in principle. But, in fact, because of very small curvature radius of the throat part (acute angle) which leads to large expansion angle for air current, the air current may separate and become a turbulent boundary layer. Foreign publications in this regard are mostly based on the laminar calculations [12,13,15,17]. However, early experiments conducted by the NOL in the United States indicated that the boundary layer in the nozzle is turbulent.

The Cohen and Reshotko[17] approximation, which has been very extensively used in boundary layer calculations in gas-dynamic laser devices in foreign countries, will be adapted. We separate it into two cases: heat conduction wall ($t_w/t_o = 0.4$) and insulated wall ($t_w/t_o = 1$). Three different ratios of specific heat ($\gamma = 1.33, 1.36, 1.4$) and five different Mach numbers ($M = 4.0, 4.25, 4.5, 4.75, 5.0$) are used to calculate parameters such as displacement thickness δ^* for a boundary layer in a nozzle which has been calculated by the Foelsch method.

Even nozzles with similar geometrical structure may develop

different boundary layers. Therefore, the displacement thickness for a nozzle boundary layer cannot be considered directly as a simplified similar parameter, but only can be expressed in a combination parameter, such as $\frac{\delta^*}{\sigma} (R_{\infty})^{1/2}$.

For convenience, we adopt a combination parameter for the displacement thickness in the form:

$$\text{DELTAPHT} = \frac{\delta^*}{h^*} \left(\frac{p_0 h^* t_0^{0.24}}{t_0^{0.2}} \right)^{1/2} = f\left(\frac{x}{h^*}, \gamma, M_E, \frac{t_0}{t_0} \right) \quad (7)$$

Once the combination parameter for displacement thickness is given, we can find the displacement thickness along the nozzle wall surface, $\delta^*(x)$, based on various given parameters, such as $\gamma, M_E, h^*, T_0, p_0, t_0/t_0$. See Figure 3.

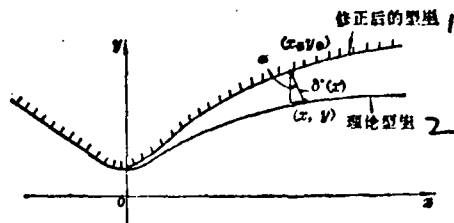


Figure 3. Boundary layer correction: 1) wall after correction; 2) theoretical wall.

The coordinates of the nozzle wall after correction is:

$$\begin{aligned} x_B &= x_n - \delta^* \sin \alpha \\ y_B &= y_n + \delta^* \cos \alpha \end{aligned} \quad (8)$$

Summary of entire calculated results leads to the following conclusions:

- 1) For given γ, M_E , and t_0/t_0 , the combination parameter DELTAPHT varies almost linearly with $\frac{x}{h^*}$. Therefore, the least square principle can be used to linearize

calculated results: $\text{DELTAPHT} = K \frac{x}{h^*}$ where K is slope.

2) For a given t_w/t_o and γ as a parameter, slope K varies with M_E approximately linearly, i.e.,

$$K(\gamma, M_E) = a(\gamma) + b(\gamma) M_E$$

where $a(\gamma)$ is the distance between the origin and the intersection of the line and axis, $b(\gamma)$ is the slope, and $a(\gamma)$ and $b(\gamma)$ are all functions of γ . In addition, $a(\gamma)$ and $b(\gamma)$ also vary approximately linearly with γ , i.e.,

$$a(\gamma) = a_0 + a_1 \gamma, b(\gamma) = b_0 + b_1 \gamma.$$

3) In terms of engineering applications, in order to satisfy the viscosity correction for a nozzle, the displacement thickness $\delta^*(x)$ can be directly added to the corresponding coordinate of the theoretical nozzle wall, i.e.,

$$x_s(x) = y_s + \delta^*(x),$$

with an error or less than 0.7%.

4) The displacement thickness of the boundary layer located at the nozzle throat, δ_r^* , is also estimated. In calculation range, δ_r^* are all small,

$$\delta_r^* < 0.0062h^*$$

In practical design, the effect of the throat boundary layer may not be considered.

Based on the foregoing considerations, tedious calcu-

lations on C-R relation including pressure variation, heat exchange, compressible boundary layer of laminar flow can be substantially simplified. It is also possible to organize the entire calculated results into approximate formulas. In a given range of parameters, all displacement thicknesses can be calculated with those formulas.

The approximate formulas for the combination parameter of displacement thickness after arrangement are:

$$\text{DELTAPHT} = \frac{\delta^*}{h^*} \left(\frac{p_0 h^* t_w^{0.24}}{t_0^{1/2}} \right)^{1/8} - K(\gamma, M_s) \frac{\delta^*}{h^*} \quad (9)$$

$$K(r, M_s) = a(\gamma) + b(\gamma) M_s = a_0 + a_1 \gamma + (b_0 + b_1 \gamma) M_s \quad (10)$$

For a laminar current heat-conduction wall, $t_w/t_o = 0.4$,

$$K \times 10^4 = 0.0088 + 0.2114\gamma + (0.1131\gamma - 0.0041) M_s \quad (11)$$

For a laminar insulated wall, $t_w/t_o = 1$,

$$K \times 10^4 = 0.7173 + 0.1054\gamma + (0.3032\gamma - 0.1667) M_s \quad (12)$$

The error introduced by the approximate formulas is less than $\pm 0.2\%$. It is generally less than ± 0.003 mm when converted to coordinates of the nozzle wall. This is tolerable in engineering.

The appropriate range for approximate formulas are:

$$\gamma = 1.33 \sim 1.4, M_s = 4 \sim 5,$$

For heat conduction wall, it is limited to $t_w/t_o = 0.4$. Nozzle coordinates are calculated by the Foelsch method.

REFERENCES

- [1] Gerry E. T.; *IEEE, Spectrum.*, 1970, **7**, 51.
- [2] Anderson J. D.; *AIAA Paper*, 69-668.
- [3] Anderson J. D.; *ACTA Astronautical*, 1975, **2**, 11.
- [4] Brunner M. J.; *AD-783218*.
- [5] Anderson J. D., Harris E. L.; *AIAA Paper 72-143*.
- [6] Greenberg R. A. et al.; *AIAA J.*, 1972, 1494.
- [7] Kuehn D. M.; *Appl. Phys. Lett.*, 1972, **21**, 3.

- [8] Yan Hai-shing, Chen Li-yin; *Chinese Journal of Mechanics*, 1978, No. 4, 274.
- [9] Foelsch K.; *North American Aviation Report No. NA-46-235*, Mar 1946.
- [10] Crown J. O.; *NACA TN-1651*.
- [11] Monder M. J.; *AIAA Paper 71-24*.
- [12] Stollery J. L., Smith J. E.; *J. of Fluid Mech.*, 1962, **18**, 225.
- [13] Sumons G. A.; *AIAA Paper, 72-709*.
- [14] Clark P. O.; *AIAA Paper, 72-708*.
- [15] Russell D. A.; *AIAA Paper, 74-223*.
- [16] Wagner J. L.; *AD-781677*.
- [17] Colon C. B., Roshko E.; *NACA Rep 1204*.

